Available online at www.sciencedirect.com
ScienceDirect
Remote Sensing of Environment 110 (2007) 186–191
Remote Sensing of Environment
www.elsevier.com/locate/rse

Detection of Asia dust storms using multisensor satellite measurements

Jianping Huang [a,*], Jinming Ge [a], Fuzhong Weng [b]

[a] College of Atmospheric Sciences, Lanzhou University, Lanzhou, China
[b] NOAA/NESDIS/Office of Research and Applications, Camp Springs, Maryland, USA

Received 4 December 2006; received in revised form 12 February 2007; accepted 17 February 2007

Abstract

Observations from visible, infrared and microwave satellite instruments are integrated to detect dust storm over northwestern China. Microwave measurements are used to detect the dust storm underneath ice clouds, while visible and infrared measurements are utilized for delineating the cloud-free dust systems. Detection is based on microwave polarized brightness temperature differences ($\Delta T_b = T_{bv} - T_{bh}$) among two channels of 89 GHz and 23.8 GHz and infrared brightness temperature difference (BTD) between channels at 11 and 12 μm. It is shown that the integrated approach is better than the method solely based on infrared BTD in storm detection, especially for those dust systems covered by ice clouds. This approach is applied for the Asia dust storms cases using the data from the Moderate Resolution Imaging Spectroradiometer (MODIS) and the Advanced Microwave Scanning Radiometer (AMSR-E) onboard Aqua satellite.

Keywords: Multisensors; Infrared measurements; Microwave measurements; Asia dust storm

1. Introduction

Mineral dust plays an important role from a climate study point of view, as do anthropogenic aerosols, especially when we consider the global trend of desertification caused by land development (Sokolik & Toon, 1996; Tegen & Lacis, 1996). The Asia dust storms most frequently originate in the regions of the Taklamakan Desert of China and the Gobi Desert of Mongolia and peak in late winter and early spring. The dust aerosol layers are capable of traveling thousands of kilometers at high altitude and outflow from the continent to the open sea near Korea and Japan under prevailing westerly conditions (Haywood et al., 1999; Higurashi & Nakajima, 2002; Takemura et al., 2002). Dust aerosol has a significant effect on the atmospheric radiation budget because of a large emission amount (Albrecht, 1989; Bréon et al., 2002; DeMott et al., 2003; Huang et al., 2006a,b; Rosenfeld & Nirel, 1996; Rosenfeld et al., 2001; Twomey et al., 1984). Such dust storms can also pose a serious health risk for people with respiratory disorders. Thus it is imperative to be able to monitor dust storms and predict their evolution.

Several techniques have been proposed for detecting mineral dust and volcanic ash using thermal–infrared observations (Ackerman, 1997; Legrand et al., 2001; Prata, 1989; Prata & Grant, 2001). Detection is based on the brightness temperature differences (BTD) either in two or three channels. Ackerman (1997) argued that a combination of three IR channels near the 8, 11, and 12 μm bands is likely to provide a more robust way to identify dust. Using satellite observations of AVHRR and HIRS/2 of dust outbreaks over the Arabian Peninsula and adjacent Arabian Sea in July 1985, Ackerman (1997) demonstrated that analyzing BTD between the 8 and 11 μm channels against BTD between the 11 and 12 μm channels enables to discriminate dust from the clear sky over both oceans and lands. However, the most common dust storms in East Asia are those caused by strong winds behind a cold front and generally coexist with cirrus. Because the visible–infrared radiance is primarily sensitive to the upper cirrus cloud layer, especially when the upper-layer cirri are thick, the BTD approach is nearly useless to detect dust under cirrus areas. The microwave radiation, however, is not significantly scattered or absorbed by ice clouds. Microwave can penetrate the ice cloud, so the change of microwave radiation caused by the dust below the cirrus can be received by the microwave sensors on satellite and finally converted to the change of brightness temperature. Consequently, it is possible to combine

* Corresponding author.
E-mail address: hjp@lzu.edu.cn (J. Huang).

0034-4257/$ - see front matter © 2007 Elsevier Inc. All rights reserved.
doi:10.1016/j.rse.2007.02.022

both visible–infrared and microwave techniques to determine the presence of a dust storm.

Little work has been done on integrated multisensors detection of dust storms. El-Askary et al. (2003, 2006) have analyzed several remote sensing instrument capabilities in monitoring dust storms and developed the multisensor approach for detecting dust storm. They have studied the behavior of dust particles at different wavelengths and found that the technique based on a combination of optical and microwave sensing is particularly useful for detecting dust storm and suggested to use scattering index (SI) which was developed by Ferraro and Grody (1994) for monitoring dust storm at microwave length.

In this paper, we proposed to use microwave polarized brightness temperature differences ($\Delta T_b = T_{bv} - T_{bh}$) combining with thermal–IR BTD approach for dust detection. The "polarization temperature difference" (PTD) at microwave frequencies was used by Greenwald et al. (1997, 1999) to estimate cloud liquid water path (LWP). It was also shown that PTD has small magnitudes over land, which is believed to be associated with land polarization, and is much less sensitive to cloud vertical location, surface temperature variability, and systematic instrumental errors. The microwave PTD is suggested to detect cloud over dust system while infrared BTD is used to monitor cloud-free dust system.

2. Data

The data used in this study are from microwave, visible and infrared measurements which are taken by Aqua satellite. Aqua is an Earth observation satellite that monitors from space various kinds of physical phenomena related to water and energy circulation. The AMSR-E is a conical scanning total power passive microwave radiometer sensing (brightness temperatures) at 6 frequencies ranging from 6.9 to 89.0 GHz. Horizontally and vertically polarized radiations are measured separately at each frequency. The AMSR-E antenna temperatures were converted to brightness temperatures T_b with the method of Wentz (1998). The MODIS has 36 spectral bands ranging in wavelength from 0.4 to 14.4 μm and is designed to remotely sense atmospheric temperature, moisture profile, clouds, aerosols, and surface properties. Fig. 1 shows an image from MODIS data for an example of dust storm cases over northwestern China. To compare the infrared and microwave brightness temperature of dust aerosol and cloud, three regions are selected to represent the dust and clouds in different environments. Box 1 (hereafter DUST) in Fig. 1 represents the cloud-free dust region. Box 2 (hereafter, CLD) denotes an area where clouds occurred in a dust-free atmosphere. Box 3 (hereafter, COD) represents overcast clouds in dusty conditions. The CLD and COD regions are selected based on observations from 701 surface meteorological stations in China and Mongolia (Wang et al., 2003). The surface stations report dust in four categories at 3-hour intervals: dust storm, wind-blown sand, floating dust, and no-dust. For a cloud region observed by satellite, if the surface observation is no-dust, this region is defined as CLD, and if the surface observation is dust storm, this region is defined as COD. For the period of 2003 to 2004, we have identified and collected six dust storm cases (see Table 1) over northwest China.

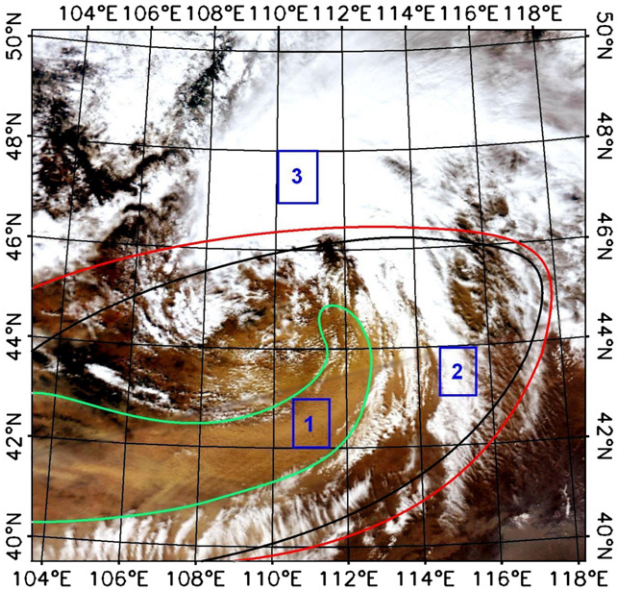

Fig. 1. Example of six dust outbreaks of the true color composite over northwest China, in which channels 0.65 μm, 0.56 μm and 0.47 μm are associated with red, green and blue colors, respectively. Box 1 is the pure dust region (DUST), box 2 the clouds over dust region (COD), and box 3 the cloud in dust-free cloud region (CLD). The regions covered by green, black, red curves are the dust areas that were decided by BTD, surface meteorological stations and multisensors method, respectively.

Table 1
Six dust cases used in this study

Image	Date	GMT	Latitude (°N)	Longitude (°E)	SAT
1	2003/03/26	04:20	38.0–48.0	118.0–132.0	Aqua
2	2003/04/09	06:15	35.0–45.0	72.0–86.0	Aqua
3	2003/04/17	07:00	35.0–45.0	73.0–87.0	Aqua
4	2004/03/09	05:30	40.0–50.0	102.0–116.0	Aqua
5	2004/03/27	05:15	40.0–50.0	104.0–118.0	Aqua
6	2004/05/08	04:15	40.0–50.0	118.0–132.0	Aqua

3. Method and results

Since channels at 11 and 12 μm lie in the thermal–IR window, absorption by other atmospheric gases is negligibly small and dust has a higher emissivity at 12 μm than at 11 μm, the BTD between the 11 and 12 μm channels (BT_{45}) can be used to detect the dust storm. Ackerman (1997) showed that the BT_{45} for dust is negative because dust has a higher albedo at 12 μm than at 11 μm. In this case, the clouds are distinct from the dust in the BT_{45} image (Fig. 2). The average BT_{45} is less than −2.0 K in the pure dust region and larger than 0 K in the cloudy regions. Using a threshold of BTD = −2 K would identify 80% of the dust. However, it can only identify 5% of pixels in the cloud over the dust region. It is because the infrared radiance is primarily sensitive to the upper cloud layer. If the threshold of −1.0 K is used for the BT_{45}, 98% of the dust can be identified and 15% of the cloud over dust can be discriminated. But in dusty areas with clouds, the BT_{45} signals tend to cancel each

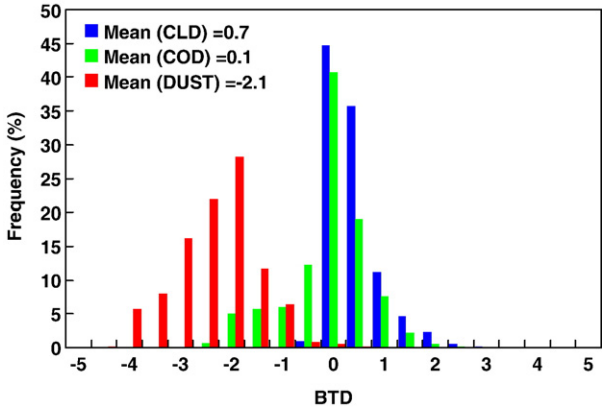

Fig. 2. Comparison of the brightness temperature difference (BTD) between 11 and 12 μm for six cases for the three regions. The blue color represents the cloud in dust-free cloud region (CLD). The red color is the pure dust region (DUST), and green the clouds over dust region (COD).

other and many pixel values of the BT_{45} in COD region are within the observed probability distribution for CLD. Thus, the discrimination cannot be possible for the dust under clouds because the BTD histograms of CLD and COD are close with peaks at 0.7 and 0.1 K, respectively. The BT_{45} can also be used as an additional constraint for detecting fire and smoke, but the threshold is $BT_{45}>4.0$ K (Li et al., 2003).

Fig. 3 compares the ΔT_b of different regions as a function of frequency for desert (Fig. 3(a)) and grassland (Fig. 3(b)) surfaces. The ΔT_b of desert is an averaged value of cases 1 and 2 listed in Table 1, while the ΔT_b of grassland surface is the mean value of cases 4 and 5 listed in Table 1. The results show that the averaged ΔT_b of COD and CLD regions is significantly different for all frequency bands. Since water droplets and precipitations can strongly reduce the differences between vertical and horizontal polarized brightness temperature, the ΔT_b values of CLD region are much smaller than those in the COD region. This suggests that the COD and CLD regions may be separated using ΔT_b for both desert and grassland surfaces. For desert surface, ΔT_b of COD region is also quite different from that in clear sky condition, the value of ΔT_b in COD region is less than that in sky condition. For grassland surface, the relationship between ΔT_b in COD region and in clear sky condition is complicated but such relationship in 89 GHz is similar to that over the desert surface.

The dimension of dust particles is larger than that of the normal aerosol particulates, but is similar to the incident wavelength of microwave radiation. Therefore, microwave radiation responds to dust particles in Mie scattering regimes. The shorter the wavelength of the incident radiation in the microwave range, the greater the scattering and hence the brightness temperature is lower (El-Askary et al., 2003). Also, the scattering in Mie regime tends to depolarize the surface polarization. Although the difference between vertically polarized channels of 23.8 and 89 GHz could represent the scattering signature of dust aerosols, water cloud and precipitation may also scatter emitted radiance and complicate the process. It is found that the simple difference between vertically polarized channels of 23.8 and 89 GHz cannot distinguish dust from the background. To overcome this shortcoming, one can use the polarized difference. As shown in Fig. 3, the slope of ΔT_b for CLD region is much smaller than that for the COD region. This suggests that the difference (ΔT_b) between lower frequency (23.8 GHz) and higher frequency (89 GHz) can be used to detect COD regions. Fig. 4 shows scatter plots of ΔT_{b89} with $\Delta T_{b23.8}$ for each of the three groups for six cases listed in Table 1. ΔT_{b89} and $\Delta T_{b23.8}$ are the difference $\Delta T_b = T_{bv} - T_{bh}$ between the vertical and horizontal components of the brightness temperature at 89 GHz and 23.8 GHz, respectively. The relationships between ΔT_{b89} and $\Delta T_{b23.8}$ are distinct for dust-free and dust groups. For CLD groups in Fig. 4, ΔT_b is small at both 89 and 23.8 frequencies and ranges from 0 to 15 K, and the mean value of ΔT_{b89} and $\Delta T_{b23.8}$ is 4.75 K and 6.05 K, respectively (see Table 2). The standard deviation of ΔT_{b89} (3.01 K) and $\Delta T_{b23.8}$ (4.18 K) is also very close. In contrast, both ΔT_{b89} and $\Delta T_{b23.8}$ are much larger for COD and DUST groups. For COD groups, mean ΔT_{b89} is 12.48 K, which is about 10.49 K less than the mean value of $\Delta T_{b23.8}$, and their standard deviations, which are 3.85 K and 6.70 K, respectively, are also quite different. In addition to the presence of clouds, this large difference arises from the fact that the MW radiation

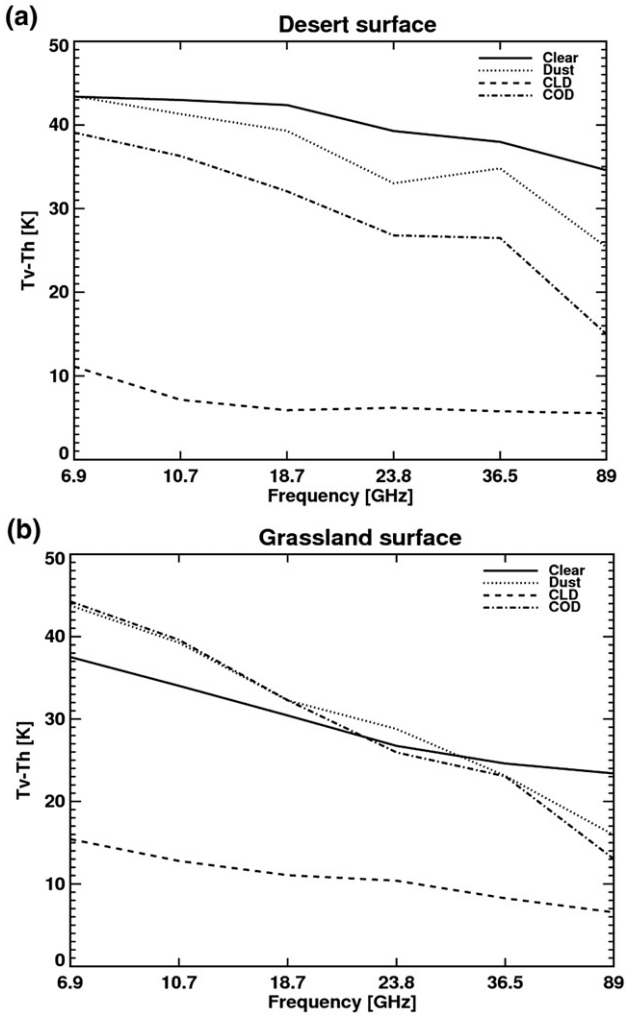

Fig. 3. The average polarized brightness temperature difference as a function of frequency for (a) desert surface and (b) grassland surface.

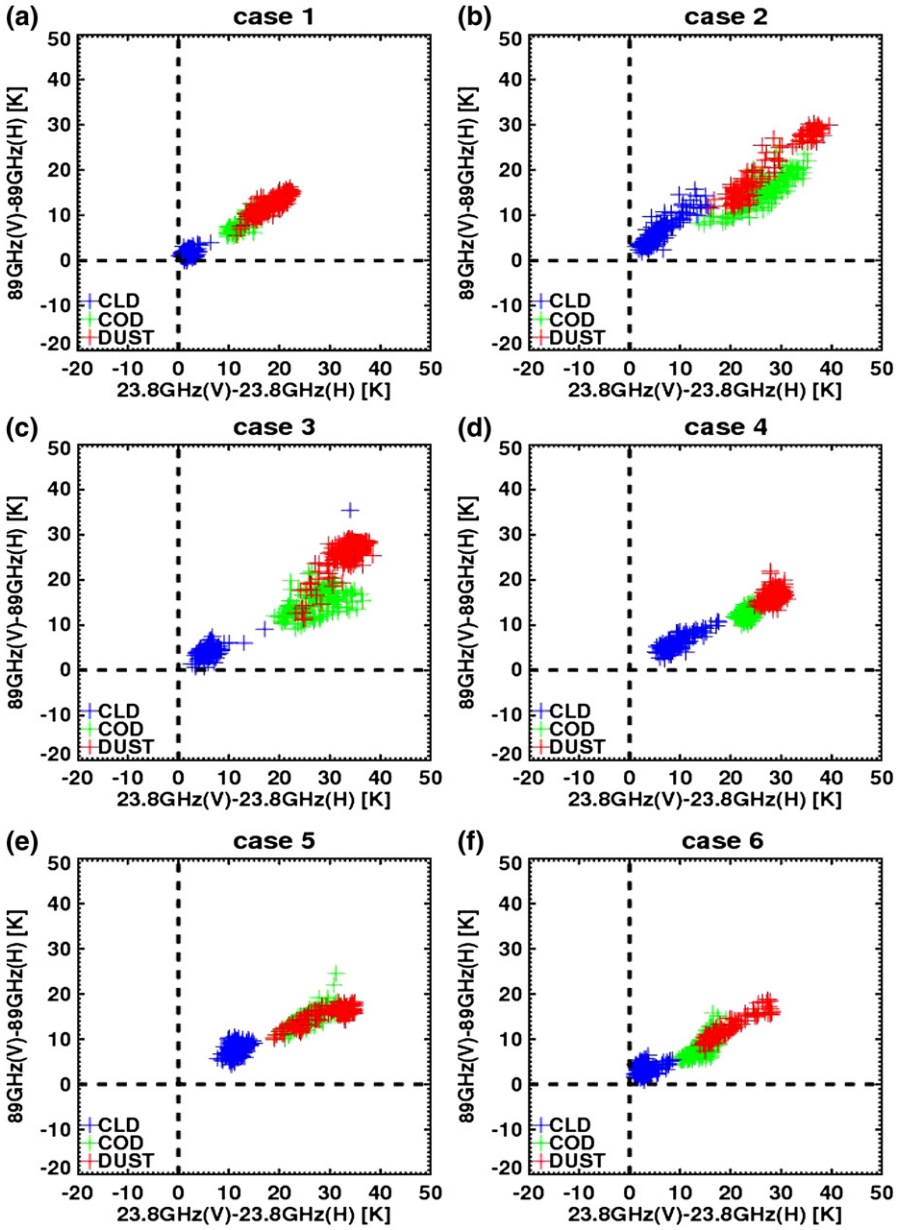

Fig. 4. Comparison of the microwave brightness temperature difference (in K) between $T_{b89v} - T_{b89h}$ and $T_{b23.8v} - T_{b23.8h}$ for six cases for the three regions. The blue color represents the cloud in the dust-free cloud region (CLD), the green the clouds over dust region (COD), and red the pure dust region (DUST).

emanates from much lower dust layers than the top ice cloud radiances. For the dust group, the mean ΔT_{b89} (20.75 K) is about 8.07 K less than the average $\Delta T_{b23.8}$ values (28.82 K), which is close to the COD group and much larger than the CLD group, their standard deviations are 6.63 K and 6.92 K, respectively. These results suggest that significant differences between ΔT_{b89} and $\Delta T_{b23.8}$ can be used as a discriminator of identifying dust storm. We define a microwave polarized index (MPI) for monitoring the dust storm. The MPI can be written as:

$$\mathrm{MPI} = \Delta T_{b89} - \Delta T_{b23.8} \quad (1)$$

Fig. 5 shows the MPI histogram for dust region (red bar), COD region (green bar) and CLD region (blue bar) which is derived from the six cases listed in Table 1. The major difference between the COD and CLD is the frequency distribution of MPI. Fig. 5 displays that better discrimination is possible for the dust under ice cloud because the MPI histograms of CLD and COD are substantially different with peaks at −1.3 and −10.5 K, respectively. However, the COD and DUST regions yield about 100% negatively large MPI

Table 2
The mean and standard deviation of the difference between vertical and horizontal components of the brightness temperature at 89 GHz and 23.8 GHz for the three regions

	CLD		COD		DUST	
	Mean	St dev	Mean	St dev	Mean	St dev
ΔT_{b89}	4.75	3.01	12.48	3.95	20.75	6.63
$\Delta T_{b23.8}$	6.05	4.18	22.97	6.70	28.82	6.92

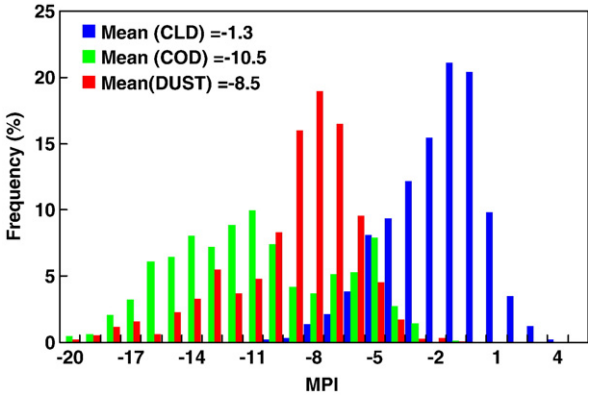

Fig. 5. Histogram of the microwave polarized brightness temperature difference index i.e., MPI=($T_{b89v}-T_{b89h}$)−($T_{b23.8v}-T_{b23.8h}$) for six cases for the three regions. The blue color represents the cloud in dust-free cloud region (CLD). The red color is the pure dust region (DUST), and green the clouds over dust region (COD).

values and their MPI histograms are relatively similar with peaks at −10.5 and −8.5 K, respectively. Using a threshold of MPI of −7.0 K, we would identify about 85% of the cloud over dust and pure dust pixels. In this case, values of MPI less than −7.0 K should indicate the presence of dust under ice cloud. However, it would misidentify 5% of the dust-free clouds having relatively small MPI (<−7.0 K). The second peak of COD may be related to areas where the dust intensities are weaker than those in pure dust regions.

Fig. 6 compares the distribution of MPI (left panel) and BTD (right panel) for the dust storm case of March 27, 2003. The coverage of red solid line is the true dust storm region determined by surface meteorological stations' observation. It can be easily seen from Fig. 6 that some cloud covered regions identified by BTD are re-identified as COD by the MPI method, and the dust storm region detected by MPI is much closer to the true dust storm region than it was identified by the BTD method. It is concluded that that discriminating dust from clouds may be possible by satellite microwave measurements. This can be achieved by only IR measurements. The combined multisensor measurements can be used to improve the determination of dust storm coverage,

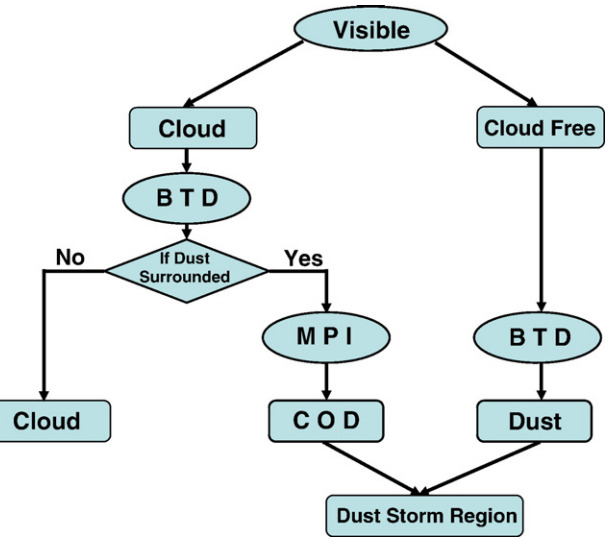

Fig. 7. Flow chart of multisensor approach for dust storms detection.

especially for detecting the COD region. Fig. 7 shows the flow chart of our multisensors approach for detecting dust storms. As it shows, the visible channel is first used to separate the target region into cloud and cloud-free regions. Then BTD method will be used to check the cloud-free region for identifying whether there exists a dust area or not. If the cloud region is surrounded by dust aerosols, the MPI method will be used to detect the dust underneath the clouds. The final dust regions, therefore, are determined by both the BTD and MPI methods. The comparison of multisensor methods with the BTD method is shown in Fig. 1. It is obvious that the dust storm coverage which is determined by the multisensor method (red curve) is much closer to the true dust storm region (black curve) than that identified by the BTD method (green curve).

4. Conclusions and discussions

BTD has been a mature method to detect pure atmospheric dust over both sea and land surfaces, but it is helpless to find the dust covered by cloud. Microwave radiation, however, can

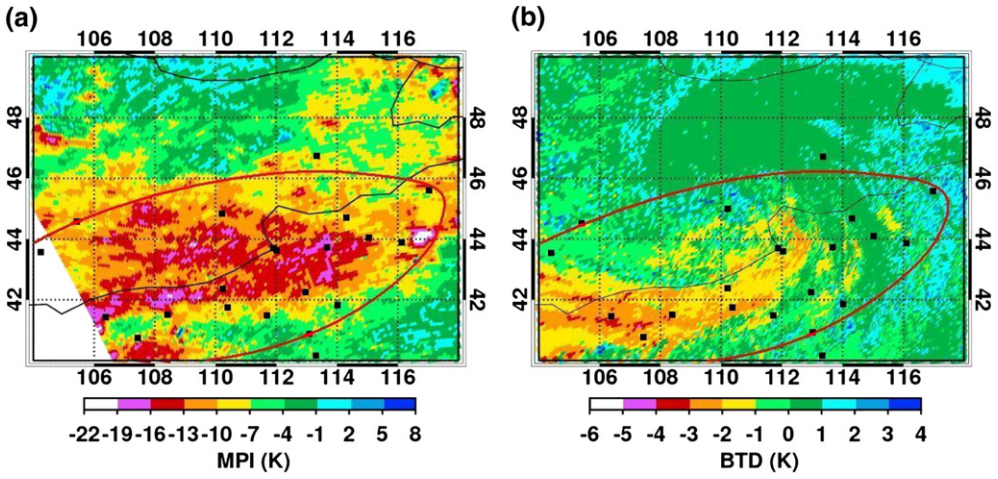

Fig. 6. Comparison of dust storm area identified by the MPI (a) and BTD (b) for the dust storm case 5 (March 27, 2004). The red solid line is the true dust storm region determined by surface observation. The surface observation sites are marked by black squares.

penetrate ice and is well suitable for monitoring dust storms when there exists an ice cloud. The method of using microwave to detect dust is based on the polarization difference technique which can partially overcome surface emissivity variability and distinguish dust from cloud. The results found here indicate that using MPI may provide accuracies of ~90% for detecting COD systems. Detection of COD with larger MPI or with better accuracy requires much additional studies. The new techniques were applied to the AMSR-E observations over northwest China. Although the techniques described in this paper exploit the AMSR-E observations, they could be easily adapted for other microwave sensor applications such as SSM/I and AMSU observations. By combining both the methods, it could be possible to overcome some of the weaknesses in the two techniques used alone. For example, the MPI data provide minimal discrimination for cloud over dust identified as ice cloud, but the BTD can be used to detect many of the pure dust regions. Conversely, the MPI is not particularly helpful in the identification of weak dust storms, but BTD appears to be useful in these cases. This approach has also a potential to discriminate dust from smoke. When dust and smoke are mixed together, the BT_{45} should be much higher than the smoke-free dust event and the BTD approach cannot discriminate the dust from the smoke. The microwave radiation, however, is not significantly scattered or absorbed by smoke. Microwave polarized brightness temperature difference can be used to detect the dust in this case.

Acknowledgments

This research is supported by the National Science Foundation of China under grant 40633017 and the National Basic Research Program of China (2006CB400501). The MODIS and AMSR-E microwave data were obtained from the NASA Earth Observing System Data and Information System, Distributed Active Archive Center (DAAC) at the GSFC.

References

Ackerman, S. A. (1997). Remote sensing aerosols using satellite infrared observations. *Journal of Geophysical Research*, *102*(D14), 17,069−17,080.

Albrecht, B. A. (1989). Aerosols, cloud microphysics, and fractional cloudiness. *Science*, *245*, 1227−1230.

Bréon, F. -M., Tanré, D., & Generoso, S. (2002). Aerosol effect on cloud droplet size monitored from satellite. *Science*, *295*, 834−838.

DeMott, P. J., Sassen, K., Poellot, M., Baumgardner, D., Rogers, D. C., Brooks, S., et al. (2003). African dust aerosols as atmospheric ice nuclei. *Geophysical Research Letters*, *30*, 1732. doi:10.1029/2003GL017410

El-Askary, H., Gautam, R., Singh, R. P., & Kafatos, M. (2006). Dust storms detection over the Indo-Gangetic basin using multi sensor data. *Advances in Space Research Journal*, *37*, 728−733.

El-Askary, H. M., Sarkar, S., & El-Ghazawi, T. A. (2003). Multisensor approach to dust storm monitoring over the Nile delta. *IEEE Transactions on Geoscience and Remote Sensing*, *41*, 2386−2391.

Ferraro, R. R., & Grody, N. C. (1994). Effects of surface conditions on rain identification using the DMSP-SSM/I. *Remote Sensing Reviews*, *11*, 195−209.

Greenwald, T. J., Combs, C. L., Jones, A. S., Randel, D. L., & Vonder Haar, T. H. (1997). Further developments in estimating cloud liquid water over land using microwave and infrared satellite measurements. *Journal of Applied Meteorology*, *36*, 389−405.

Greenwald, T. J., Combs, C. L., Jones, A. S., Randel, D. L., & Vonder Haar, T. H. (1999). Error estimates of spaceborne passive microwave retrievals of cloud liquid water over land. *IEEE Transactions on Geoscience and Remote Sensing*, *37*, 796−804.

Haywood, J. M., Ramaswamy, V., & Soden, B. J. (1999). Tropospheric aerosol climate forcing in clear-sky satellite observations over the oceans. *Science*, *283*, 1299−1305.

Higurashi, A., & Nakajima, T. (2002). Detection of aerosol types over the East China Sea near Japan from four-channel satellite data. *Geophysical Research Letters*, *29*, 1836. doi:10.1029/2002GL015357

Huang, J., Lin, B., Minnis, P., Wang, T., Wang, X., Hu, Y., et al. (2006). Satellite-based assessment of possible dust aerosols semi-direct effect on cloud water path over East Asia. *Geophysical Research Letters*, *33*. doi:10.1029/2006GL026561

Huang, J., Minnis, P., Lin, B., Wang, T., Yi, Y., Hu, Y., et al. (2006). Possible influences of Asian dust aerosols on cloud properties and radiative forcing observed from MODIS and CERES. *Geophysical Research Letters*, *33*, L06824. doi:10.1029/2005GL024724

Legrand, M., Plana-Fattori, A., & N'Doume', C. (2001). Satellite detection of dust using the IR imagery of Meteosat, 1, infrared difference dust index. *Journal of Geophysical Research*, *106*, 18,251−18,274.

Li, Z., Fraser, R., Jin, J., Abuelgasim, A. A., Csiszar, I., Gong, P., et al. (2003). Evaluation of algorithms for fire detection and mapping across North America from satellite. *Journal of Geophysical Research*, *108*(D2), 4076. doi:10.1029/2001JD001377

Prata, A. J. (1989). Observations of volcanic ash clouds in the 10−12 micrometer window using AVHRR/2 data. *International Journal of Remote Sensing*, *10*, 751−761.

Prata, A. J., & Grant, I. F. (2001). Retrieval of microphysical and morphological properties of volcanic ash plumes from satellite data: Application to Mt. Ruapehu, New Zealand. *Quarterly Journal of the Royal Meteorological Society*, *127*, 2153−2179.

Rosenfeld, D., & Nirel, R. (1996). Seeding effectiveness — The interaction of desert dust and the southern margins of rain cloud systems in Israel. *Journal of Applied Meteorology*, *35*, 1502−1510.

Rosenfeld, D., Rudich, Y., & Lahav, R. (2001). Desert dust suppressing precipitation: A possible desertification feedback loop. *Proceedings of the National Academy of Sciences*, *98*(11), 5975−5980.

Sokolik, I. N., & Toon, O. B. (1996). Direct radiative forcing by anthropogenic mineral aerosols. *Nature*, *381*, 681−683.

Takemura, T., Uno, I., Nakajima, T., Higurashi, A., & Sano, I. (2002). Modeling study of long-range transport of Asian dust and anthropogenic aerosols from East Asia. *Geophysical Research Letters*, *107*, 2158. doi:10.1029/2002GL016251

Tegen, I., & Lacis, A. A. (1996). Modeling of particle size distribution and its influence on the radiative properties of mineral dust aerosol. *Journal of Geophysical Research*, *101*, 19237−19244.

Twomey, S., Piepgrass, M., & Wolfe, T. L. (1984). An assessment of the impact of pollution on global cloud albedo. *Tellus*, *36B*, 356−366.

Wang, S., Wang, J., Zhou, Z., Shang, K., Yang, D., & Zhao, Z. (2003). Regional characteristics of dust events in China. *Journal of Geographical Sciences*, *13*, 35−44.

Wentz, F. J. (1998). *Algorithm theoretical basis document: AMSR ocean algorithm.* Remote Sensing Systems Tech. Rep. 110398, Santa Rosa, CA 28 pp.

Further reading

Ackerman, A. S., Toon, O. B., Stevens, D. E., Heymsfield, A. J., Ramanathan, V., & Welton, E. J. (2000). Reduction of tropical cloudiness by soot. *Science*, *288*, 1042−1047.

Levi, Y., & Rosenfeld, D. (1996). Ice nuclei, rainwater chemical composition, and static cloud seeding effects in Israel. *Journal of Applied Meteorology*, *35*, 1494−1501.